

See discussions, stats, and author profiles for this publication at: <https://www.researchgate.net/publication/231376194>

Dissipative Particle Dynamics and Flory –Huggins Theories for Predicting the Rheological Behavior of Ultrahigh Molecular Weight Polyethylene Blends

ARTICLE *in* INDUSTRIAL & ENGINEERING CHEMISTRY RESEARCH · OCTOBER 2010

Impact Factor: 2.59 · DOI: 10.1021/ie100959f

CITATIONS

4

READS

30

5 AUTHORS, INCLUDING:



[Guo-Hua Hu](#)

University of Lorraine

212 PUBLICATIONS 4,111 CITATIONS

[SEE PROFILE](#)



[Sandrine Hoppe](#)

University of Lorraine

55 PUBLICATIONS 309 CITATIONS

[SEE PROFILE](#)

Dissipative Particle Dynamics and Flory–Huggins Theories for Predicting the Rheological Behavior of Ultrahigh Molecular Weight Polyethylene Blends

Jing-Gang Gai,^{†,‡} Guo-Hua Hu,^{*,‡,§} Hui-Lin Li,^{*,†} Shi-Peng Zhu,[†] and Sandrine Hoppe^{*}

State Key Laboratory of Polymer Materials Engineering, Polymer Research Institute of Sichuan University, Chengdu, Sichuan 610065, China, Laboratory of Reactions and Process Engineering, CNRS-Nancy Université-ENSIC-INPL, 1 rue Grandville, BP 20451, 54001 Nancy, France, and Institut Universitaire de France, Maison des Universités, 103 Boulevard Saint-Michel, 75005 Paris, France

This work aims to experimentally and theoretically study the effects of normal molecular weight polymers (NMWP) such as high-density polyethylene, low-density polyethylene, and polypropylene as processing aids on the morphology and rheological behavior of ultrahigh molecular weight polyethylene (UHMWPE). As is shown by scanning electron microscope observations, rheological measurements, and dissipative particle dynamics simulations, formation of a lubricating phase between the UHMWPE particles is responsible for the viscosity reduction of the UHMWPE. Besides, phase diagram studies on the UHMWPE/NMWP blend suggest that the optimum composition ratio of the blends lies in their composition-sensitive region when the parameter χ and molecular weight of each component are fixed at low shear rates. Meanwhile, the optimum range of parameter χ is above but close to the corresponding binodal curve at high shear rates.

1. Introduction

UHMWPE and its composites are widely used as bearing components, ballistic dresses, and medical materials in total joint replacement^{1–3} because of their outstanding friction and wear characteristics, biocompatibility, chemical resistance, and mechanical properties.^{4,5} Unfortunately, the extremely high melt viscosity of UHMWPE due to its extremely high molecular weight makes it hard to be processed by conventional melt processes such as extrusion and injection molding.

The development of high-performance UHMWPE material often has to call upon the use of a low molecular weight solvent to reduce its high viscosity. For example, a so-called “gel-spinning process” used for the industrial production of high-strength UHMWPE fibers requires a large amount of solvents, which often exceeds 100–1000 times the volume of the resulting UHMWPE fibers and is difficult to remove and recycle.^{6,7} Therefore, much attention has been paid to solvent-free processes for reactor powder drawing.

An alternative route to reduce the melt viscosity is to mix UHMWPE with NMWP like high-density polyethylene (HDPE),⁸ low-density polyethylene (LDPE),⁹ polypropylene (PP),¹⁰ polyethylene glycol (PEG),¹¹ and polylactic acid (PLA).¹² The advantage of this method lies in its dry processing. Conventional polyethylenes (HDPE, LDPE, and LLDPE) are the most commonly used NMWP. It was found that melt flowabilities of UHMWPE blends could be improved with increasing the contents of these conventional polyethylenes,¹³ but the viscosity of UHMWPE/HDPE was the highest when equal contents of the conventional polyethylenes were added. Cocrystallization took place in the blends of UHMWPE/LLDPE and UHMWPE/HDPE; meanwhile, separate crystals were formed in UHMWPE/LDPE. The tensile properties of the former two blends varied almost linearly with blend composition, while

deviations were seen in the latter UHMWPE/LDPE. Besides, rheological and mechanical properties of the UHMWPE blends were profoundly affected by the mixing process. Vadhar et al.⁹ adapted two mixing techniques (namely, simultaneous and subsequent loading methods) to study the properties of UHMWPE/LLDPE blend. The results showed LLDPE could effectively reduce the UHMWPE viscosity for the two mixing processes, but the sequential loading method provided more homogeneous compounds than those of simultaneous blending. Tensile properties of subsequent loading blend varied more or less linearly with blend compositions, whereas negative and positive deviations were seen in the simultaneously prepared blends.

Other types of NMWP have also been investigated. Mixed with 10–30% polypropylene (PP), UHMWPE could be extruded by a conventional single extruder.¹⁴ Its mechanical and tribological properties were as good as or even better than those of the pure UHMWPE. Further reduction in viscosity of the blend was obtained by the incorporation of 1 phr PEG.¹¹ PLA was also used to improve the melt flowability of UHMWPE.¹² It was found that there appeared to be a remarkable decrease in melt viscosity, an improvement in dimension stability, and a reduction in tensile yield strength and notched impact strength of the UHMWPE/PLA blend with the increase of the PLA content. When PLA content was about 10%, the blend not only retained its attributes like original notched impact strength and ductile fracture but also possessed good melt flow properties.

Numerous studies indicate that adding certain NMWP to UHMWPE could significantly change the viscosity of the latter while retaining even enhancing its mechanical properties under certain conditions. The various UHMWPE/NMWP blends studied differed from each other in the interaction parameter χ , molecular weight, and content of each component. However, none of those studies reported on the optimum windows for these parameters within which the viscosity of UHMWPE can be significantly reduced while its mechanical properties retained.

Presently, it is common to use experimental approaches to study the viscosity reduction mechanism and the optimization of parameter ranges. However, it is not always possible to study all UHMWPE/NMWP blends upon varying thoroughly param-

* To whom correspondence should be addressed. G.-H.H.: tel., +33 383175339; fax, +33 383322975; e-mail, hu@ensic.inpl-nancy.fr. H.L.L.: tel., +86 28 85406333; fax, +86 28 85402465; e-mail, nic7703@scc.edu.cn.

[†] Polymer Research Institute of Sichuan University.

[‡] CNRS-Nancy Université-ENSIC-INPL.

[§] Maison des Universités.

eters like interaction parameter χ , molecular weight, and content of each component. Therefore, theoretical calculations are necessary.

The dissipative particle dynamics (DPD) method developed by Hoogerbrugge and Koelman^{15,16} is a mesoscopic simulation technique for complex fluids and can be used to study systems over larger length and time scales than classical molecular dynamics. Español and Warren added the fluctuation–dissipation relation in DPD.¹⁷ Together with Groot, they also applied a coarse-grained method to build a mapping relation of force parameters in DPD with the energy parameters in Flory–Huggins theory.¹⁸ Besides, refs 19–22 showed that DPD simulations could quantitatively predict some of the properties of the real systems. This method is particularly suitable for studying the phase separation and rheological properties of block copolymers and polymer blends.^{19,23,24}

In this study, the microscopic morphologies, mixing kinetics, and rheological behaviors of binary UHMWPE/PP, UHMWPE/LDPE, and UHMWPE/HDPE blends are studied by the DPD simulations, SEM observations, and rheological measurements. On the basis of these results, a possible mechanism responsible for viscosity reduction is proposed. Besides, phase diagrams calculated from Flory–Huggins theory are adopted here to investigate the effects of interaction parameter χ , molecular weight, and content of each component on the microscopic morphologies, mixing kinetics, and viscosity of blends. Moreover, optimum parameter ranges for processing UHMWPE are also assessed both experimentally and theoretically.

2. Experimental Section

2.1. Materials. UHMWPE (M-II), with an average viscosity molecular weight of 2.5×10^6 and a mean particle diameter of about $300 \mu\text{m}$, was supplied by Beijing No. 2 Auxiliary Agent Factory (Beijing, China). HDPE (6098) and PP (F401) were supplied by Shandong Qilu Petrochemical Engineering Co., Ltd. (Shandong, China) and Lanzhou Chemical Industry Factory (Lanzhou, China) with a melt flow rate (MFR) of $2.0 \text{ g}/10 \text{ min}$ (230°C , 2.16 kg load). LDPE (2426K) with 20–28 branches/1000 long chain carbons was also supplied by Lanzhou Chemical Industry Factory (Lanzhou, China). NMWP denotes the polymer, whose average molecular weight is far less than that of UHMWPE, such as LDPE, HDPE, and PP.

2.2. UHMWPE Blend Preparation. A general-purpose three-section single-screw extruder ($D = 25 \text{ mm}$, $L/D = 25$) with a circular die was used to prepare UHMWPE blends. The temperatures for all sections and the die were 230°C . Extrudates were pelletized and compression molded to 4 mm plates for subsequent scanning electron microscope (SEM) observations.

2.3. Rheological Experiments. A capillary rheometer of type Gottfert Rheograph 2002 (Gottfert Co., Germany) was used. Its capillary diameter and length-to-diameter ratio were 1 mm and 30 . The die had an entrance angle of 180° . Considering the long length-to-diameter ratio, entrance pressure losses were assumed to be negligible and consequently no Bagley corrections were made. The flow properties of the UHMWPE blends were measured at 230°C .

2.4. Morphological Characterization. A scanning electron microscope of type JSM 5900 LV, Tokyo, Japan, was used to observe the morphology of UHMWPE/PP blends. Before the SEM observation, specimens were prepared by fracture in liquid nitrogen. The fractured surfaces were immersed in a solution of 1.3 wt \% KMnO_4 dissolved in a $\text{H}_2\text{SO}_4/\text{H}_3\text{PO}_4/\text{H}_2\text{O}$ (10/4/1) mixture in order to etch out the amorphous phase.

3. Theoretical Background

3.1. Phase Diagram. The F–H expression for the free energy density of mixing of component 1 with component 2 is given by^{25–28}

$$\frac{F_{\text{mix}}}{k_{\text{B}}T} = \frac{\phi_1 \ln \phi_1}{N_1} + \frac{\phi_2 \ln \phi_2}{N_2} + \chi \phi_1 \phi_2 \quad (1)$$

where k_{B} is the Boltzmann constant, T is the absolute temperature, ϕ_i and N_i are the volume fractions and numbers of segments per molecule, and χ is the interaction parameter. An implicit condition associated with this equation is that the lattice is filled completely, namely, $\phi_1 + \phi_2 = 1$. Under this condition, $\phi_2 = 1 - \phi_1$, with ϕ_1 being the only degree of freedom. The first two terms on the right of eq 1 represent the combinatorial entropies for random mixtures of chain molecules, while the last term provides pairwise interactions between randomly mixed chain units.

A phase diagram can be constructed to summarize the phase behavior of the mixture, showing regions of stability, instability, and metastability. The binodal curve is determined by the common tangent of the free energy at compositions ϕ^{I} and ϕ^{II} corresponding to the two equilibrium phases

$$\left(\frac{\partial F_{\text{mix}}}{\partial \phi} \right)_{\phi=\phi^{\text{I}}} = \left(\frac{\partial F_{\text{mix}}}{\partial \phi} \right)_{\phi=\phi^{\text{II}}} \quad (2)$$

i.e., the curve is calculated by simultaneously solving the following two equations

$$\begin{aligned} \ln \left(\frac{\phi_1^{\text{I}}}{\phi_1^{\text{II}}} \right) + (\phi_1^{\text{II}} - \phi_1^{\text{I}})(1 - N_1/N_2) + \\ \chi N_1[(1 - \phi_1^{\text{I}})^2 - (1 - \phi_1^{\text{II}})^2] = 0 \end{aligned} \quad (3)$$

$$\begin{aligned} \ln \left(\frac{1 - \phi_1^{\text{I}}}{1 - \phi_1^{\text{II}}} \right) + (\phi_1^{\text{I}} - \phi_1^{\text{II}})(1 - N_2/N_1) + \\ \chi N_2[(\phi_1^{\text{I}})^2 - (\phi_1^{\text{II}})^2] = 0 \end{aligned} \quad (4)$$

where ϕ_1^{I} and ϕ_1^{II} are the volume fractions of polymer 1 in the two coexisting phases labeled I and II.

The spinodal curve defines the boundary between unstable and metastable mixtures. Thermodynamically, the spinodal condition is defined by

$$\partial^2 F_{\text{mix}} / \partial \phi^2 = 0 \quad (5)$$

3.2. DPD Simulation. In the DPD simulation, the time evolution of motion for a set of interacting particles is solved by Newton's equation¹⁸

$$\frac{d\mathbf{r}_i}{dt} = \mathbf{v}_i, \quad \frac{d\mathbf{v}_i}{dt} = \mathbf{f}_i \quad (6)$$

where \mathbf{r}_i and \mathbf{v}_i are the position and velocity of the i th particle. In this method, the force acting on a particle contains three pairwise additive parts

$$\mathbf{f}_i = \sum_{j \neq i} (\mathbf{F}_{ij}^{\text{C}} + \mathbf{F}_{ij}^{\text{D}} + \mathbf{F}_{ij}^{\text{R}}) \quad (7)$$

where \mathbf{F}^{C} , \mathbf{F}^{D} , and \mathbf{F}^{R} represent conservative, dissipative, and random forces, respectively. The sum runs over all other particles within a certain cutoff radius r_c . As this is the only length scale in the system, the cutoff radius is always used as

the unit of length, $r_c = 1$. The different parts of the forces are given by

$$\mathbf{F}_{ij}^C = \begin{cases} a_{ij}(1 - r_{ij})\mathbf{e}_{ij} & r_{ij} < 1 \\ 0 & r_{ij} \geq 1 \end{cases} \quad (8)$$

$$\mathbf{F}_{ij}^D = -\gamma\omega^D(r_{ij})(\mathbf{e}_{ij} \cdot \mathbf{v}_{ij})\mathbf{e}_{ij} \quad (9)$$

$$\mathbf{F}_{ij}^R = \sigma\omega^R(r_{ij})\xi_{ij}\Delta t^{-1/2}\mathbf{e}_{ij} \quad (10)$$

where $\mathbf{r}_{ij} = \mathbf{r}_i - \mathbf{r}_j$, $r_{ij} = |\mathbf{r}_{ij}|$, $\mathbf{e}_{ij} = \mathbf{r}_{ij}/r_{ij}$, and $\mathbf{v}_{ij} = \mathbf{v}_i - \mathbf{v}_j$. ξ_{ij} is a random number with zero mean and unit variance. a_{ij} is a constant which describes the maximum repulsion between interacting beads. ω^D and ω^R stand for r -dependent weight functions for the dissipative and random forces, respectively, and they vanish for $r > r_c = 1$. The physical interpretation of the dissipative force is as follows. If $(\mathbf{e}_{ij} \cdot \mathbf{v}_{ij}) > 0$, it means that particle i is moving apart from j and, therefore, it feels a viscous force toward j . If it moves toward j the viscous force is in the opposite direction. The random forces \mathbf{F}^R which are also radially directed provide the continuous kicks that keep the system in thermal motion. These kicks do satisfy Newton's third law and then conserve the total momentum. The dissipative force \mathbf{F}^D and the random force \mathbf{F}^R act as heat sink and source, respectively, so their combined effect is a thermostat. Espanol and Warren have shown that there is the following fluctuation–dissipation theorem in the dissipative force and the random force¹⁷

$$\omega^D(r) = [\omega^R(r)]^2\sigma^2 = 2\gamma k_B T \quad (11)$$

The weight functions are chosen simply by¹⁸

$$\omega^D(r) = [\omega^R(r)]^2 = \begin{cases} (1 - r)^2 & r < 1 \\ 0 & r \geq 1 \end{cases} \quad (12)$$

For detailed information, refer to Groot and Warren's work.¹⁸

The soft-sphere interactions of DPD can be mapped onto Flory–Huggins theory through the χ parameter.^{18,19} If the system has i and j components or beads interacting with each other and if one chooses $a_{ii} = a_{jj}$ and assumes that $\rho_i + \rho_j$ is approximately constant, then, according to Groot and Warren,¹⁸ the mapping relation is

$$\chi = \frac{2\alpha(a_{ij} - a_{ii})(\rho_i + \rho_j)}{k_B T} \quad (13)$$

where α is a parameter related to the pair-correlation function $g(r)$, which is expressed as a function of the reduced coordinate $r = \mathbf{r}/r_c$, and $\rho_i + \rho_j = \rho$ is the density of the system. The conservative interaction strength α_{ij} was chosen according to the linear relation with Flory–Huggins χ parameters for polymers¹⁸

$$\alpha_{ij} = \alpha_{ii} + 3.27\chi_{ij}(\rho = 3) \quad (14)$$

The interaction parameter between the same type beads α_{ii} equals 25. In the present study, we estimated χ of UHMWPE/PP pairs from the solubility parameters using eq 15²⁹

$$\chi = \frac{V_{\text{bead}}(\delta_i - \delta_j)^2}{RT} \quad (15)$$

where V_{bead} is the average molar volume of the beads and δ_i and δ_j are the solubility parameters of beads i and j , respectively.³⁰

In DPD, all properties are reported in the reduced units m , r_c , and $k_B T$ or combinations thereof. To relate the results of a simulation to a physical system requires substitution of the values of m , r_c , and $k_B T$ for the appropriate physical units. Having specified the reduced units, all derived properties can be calculated. If n is the numbers of time steps and Δt is time step in reduced units, the extrusion time in physical units is $t = n\Delta t r_c(m/k_B T)^{0.5}$. The DPD simulations of the UHMWPE/NMWP blends were performed in a cell of size $30 \times 30 \times 30$, with the bead density $\rho = 3$. Periodic boundary conditions were applied, and the shear flow was simulated by means of Lees–Edwards boundary conditions. For convenience, the particle mass m and $k_B T$ were all taken as unit. The time step Δt was taken as 0.05,³¹ and adjacent particles in the polymer chain interacted via a linear spring with a harmonic spring constant of 4.0, according to Groot and Liu.^{32–35} Besides, the friction coefficient γ was chosen as 4.5.³⁵

Figure 1 shows that the as-received M-II powders are made of large particles with an average diameter of about $300 \mu\text{m}$. Those large particles were in turn made of small ones of about $10 \mu\text{m}$ in diameter. Those small ones were aggregates of yet smaller, submicrometer particles. This work focuses not only on the thermodynamic properties but also on the mixing kinetics of blends. Compared with UHMWPE, it is easier to plasticize NMWP. Therefore, UHMWPE is initially encapsulated by NMWP. This core–shell configuration is the starting point of the DPD simulations and is called the core–shell initial configuration. Another configuration is that UHMWPE and NMWP are initially randomly mixed and is called random initial configuration.

The number of beads in each mesoscale molecule is determined by the degree of polymerization and the characteristic ratio (C_n) of the polymer. The expression for the DPD chain length (N_{DPD}) is³⁶

$$N_{\text{DPD}} = \frac{M_p}{M_m C_n} \quad (16)$$

where M_p is the polymer molar mass, M_m is the monomer molar mass, and C_n is the characteristic ratio. The characteristic ratio tends to be greatly affected by the determination method. As is stated in ref 37, depending on different determination methods, the characteristic ratio for PE can be varied from 6.4 to 10.3. To minimize the difference, the characteristic ratio for all polymers is measured by the same method of quantitative structure–property relationship (QSPR) in our work.³⁸ Table 1 shows the characteristic ratios, molar masses, and corresponding DPD chain lengths of the species in the UHMWPE/NMWP blends.

4. Results and Discussion

4.1. Morphology of the UHMWPE/NMWP Binary Blends.

Generally speaking, the rheological behavior of polymer blends strongly depends on their mesoscopic structure in the melt state.^{39,40} In this section, DPD simulations are used to study the effects of the parameter χ and the volume fraction of NMWP on the mesoscopic morphology and the rheological behavior of mixing of the blends of the UHMWPE with HDPE ($\chi = 0$), PP ($\chi = 9 \times 10^{-3}$), and LDPE. The measured χ values for PE blends with small differences in branch contents < 30 from SANS are usually less than 6×10^{-4} .⁴¹ The effects of PP, LDPE, and HDPE on the rheological behaviors and structures of UHMWPE are compared to study the relationship between the rheological behaviors and the structures of the UHMWPE/NMWP blends

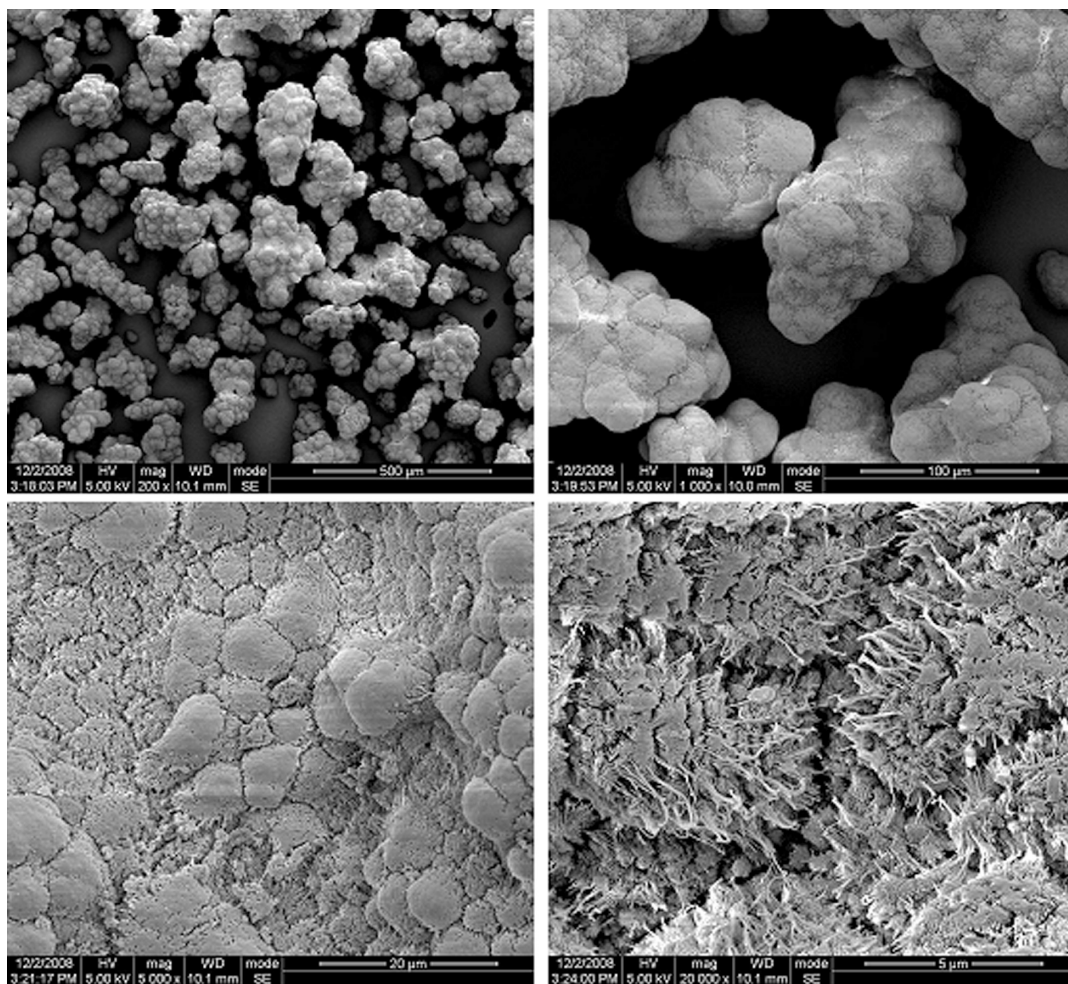


Figure 1. SEM of UHMWPE powder.

Table 1. Characteristic Ratios, Molar Masses, and Corresponding DPD Chain Lengths of the Polymer Components Involved in the UHMWPE Blends

polymer components	M_p	C_n	N_{DPD}
UHMWPE	2.5×10^6	7.7	11 600
PP	7.3×10^4	6.9	250
HDPE	5.4×10^4	7.7	250

and explore their mechanism of viscosity reduction. For the sake of comparability, equal compositions of the three blends have been adopted in our investigation.

4.1.1. UHMWPE/HDPE Blends. Figure 2 shows the SEM micrographs of the cryogenically fractured surfaces at two magnifications of UHMWPE, HDPE, UHMWPE/HDPE (50/50), and UHMWPE/PP (50/50) blends with the amorphous phase etched. UHMWPE shows the characteristic fibril-like crystal morphology (Figure 2a). Figure 2a–c indicates that the pure UHMWPE and HDPE crystal domains could not be distinguished in the UHMWPE/HDPE (50/50) blend, and the blend shows homogeneous phases.

The DPD simulation is also used to study the equilibrium state morphology of the UHMWPE/HDPE (50/50) blend. First, the effects of the initial configuration of the blend on the equilibrium state morphology are studied by comparing the morphologies originated from the random and core–shell initial configurations shown in Figures 3a and 4a. Both Figures 3b and 4h show that all the morphologies resulting from these two initial configurations are homogeneous phases, suggesting that

the simulation time together with 2.5×10^4 steps is enough to obtain the equilibrium state structure of the UHMWPE/HDPE (50/50) blend. This is in agreement with the SEM observations.

The DPD simulations were used to evaluate the evolution of the morphology with time for the UHMWPE/HDPE blend. The one with a composition of 50/50 was taken as an example. Figure 4 shows snapshots of the morphologies of the blend in the evolution process. Figure 4a–d shows an obvious increase in the interface thickness, confirming good miscibility between the two polymers. For Figure 4e, the high-density region ($\rho \geq 2.000$ DPD units) of the HDPE has almost disappeared whereas that of the UHMWPE remains relatively important in the blend. As shown in Figure 4g, both the interface and the high-density region of the UHMWPE vanish, and the UHMWPE/HDPE (50/50) blend approximately possesses a homogeneous phase after 1.1×10^4 time steps. Then this structure evolves very little with time. Finally, the blend reaches a homogeneous phase in Figure 4h. The homogeneous phase morphology of the UHMWPE/HDPE (50/50) blend is also corroborated by its density profile. There is virtually no fluctuation in density distributions for UHMWPE and HDPE after 1.1×10^4 time steps (Figure 5).

4.1.2. UHMWPE/PP Blends. The morphology of the etched cryogenically fractured surfaces of the UHMWPE/PP (50/50) blend shows many blocks (Figure 2d). Those dispersed blocks are similar to those of the pure UHMWPE and correspond to the crystalline domains of the UHMWPE in the blend. Besides, the large particles of the as-received UHMWPE powder (Figure 1) were dispersed in the PP phase in the form of aggregates. In

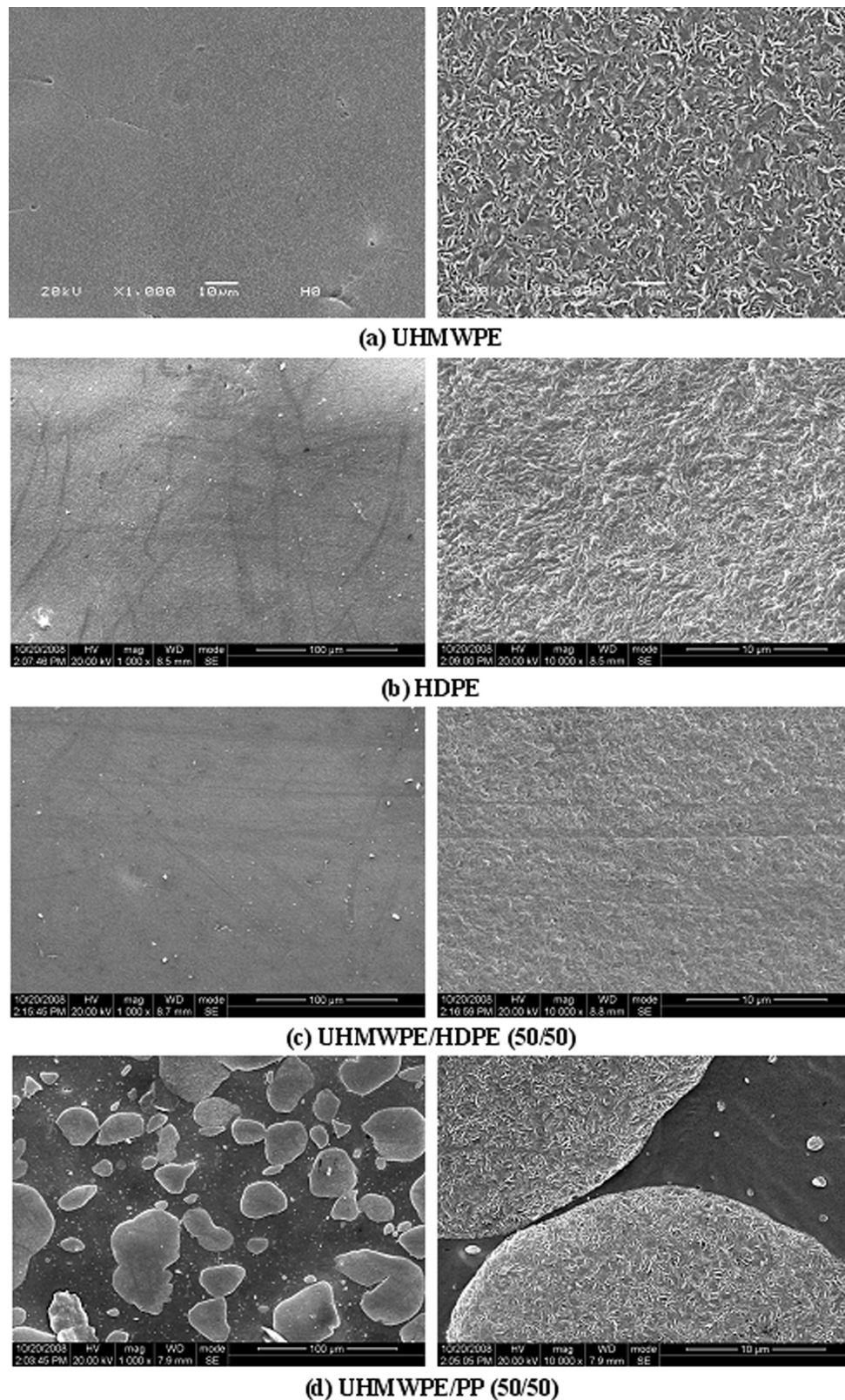


Figure 2. SEM micrographs of cryogenically fractured surfaces after etching.

other words, aggregates are coated and consequently lubricated by the PP phase and the blend shows two-phase structure.

Both the core–shell and the random initial configurations are also adopted in the DPD simulations for the UHMWPE/PP (50/50) blend. As shown in Figure 6, the resulting morphologies of the blend corresponding to the two initial configurations are both of two-phase structure. This suggests that the simulation

time with 4×10^5 steps is enough to obtain the equilibrium state of the UHMWPE/PP (50/50) blend.

Figure 7 shows the effect of the composition of the PP on the mesoscopic morphology of the UHMWPE/PP blend corresponding to 4×10^5 time steps of DPD simulation. From Figure 7a, adding 5% PP to the UHMWPE seemingly leads to a totally disordered and homogeneous phase. Between the totally dis-

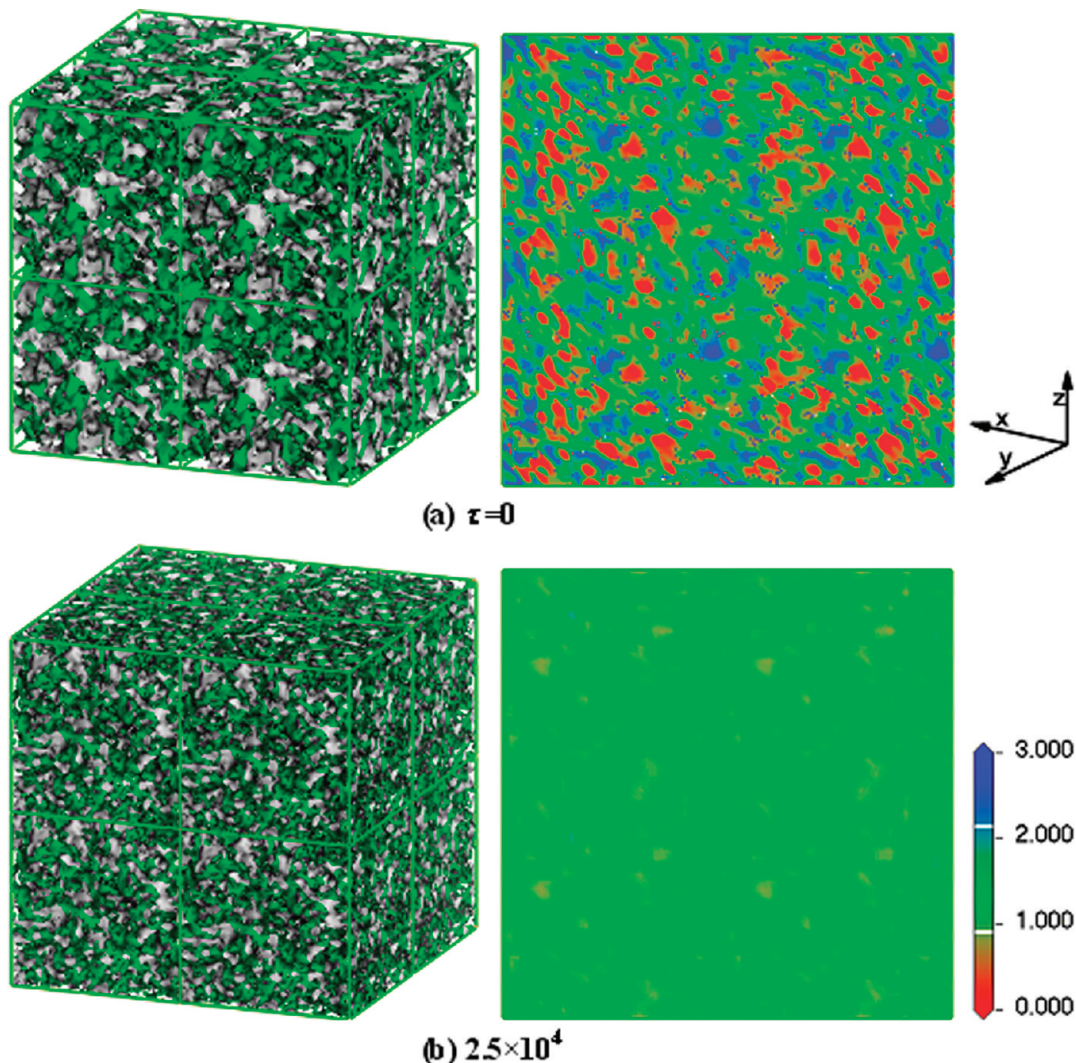


Figure 3. Snapshots of the UHMWPE/HDPE (50/50) blend simulated from a random initial configuration. (Left) Time evolution of the isodensity surfaces of the HDPE. The outward surfaces of the HDPE phases are colored green, and the rest are UHMWPE phases. (Right) Corresponding slices perpendicular to the y axis (the legend shows the magnitudes of density in the slices denoted by different colors that vary from 0.000 to 3.000); the high-density region of the UHMWPE are colored red; the isodensity line of the UHMWPE for $\rho(\text{UHMWPE}) = 0.900$ and 2.100 is colored white. τ is the time step of simulation.

ordered region and the ordered phases there are some micelle-like structures. There is no symmetry in the phases. Therefore, the ordered phases can be described as droplets (whatever their size) of the minor phase dispersed in disordered phases.^{19,32} Micelle-like phases are found in the UHMWPE/PP (90/10) blend (Figure 8b). When ϕ_{PP} (volume fraction of PP) exceeds 0.2, two-phase structures with various morphologies are observed (Figure 7c and 7d).

4.2. Mechanisms of the Viscosity Reduction for UHMWPE/NMWP Blends. Figure 8 shows the effects of the PP, LDPE, and HDPE on the rheological properties of the UHMWPE. No reliable rheological data were obtained with the pure UHMWPE and UHMWPE/HDPE (50/50) blends because they had difficulties with flow in the capillary rheometer. This was corroborated by the fact that the extrusion of the UHMWPE/HDPE (50/50) blend was very difficult. The fact that the presence of the HDPE did not improve the flow characteristics of the UHMWPE to a sufficient extent was because of the good miscibility between them. As shown in Figure 4, with increasing plasticating time and the molten HDPE rapidly penetrating the UHMWPE domains, less and less HDPE melt exists in the skin of the blend and between the UHMWPE particles and the striation thickness which represents the HDPE phase significantly decreasing. Owing to the weakening of lubricating effect

of HDPE phase on the UHMWPE particles, the melt viscosity of the UHMWPE/HDPE blend increases remarkably.

It is remarkable to note that addition of PP in UHMWPE effectively solves the above-mentioned flow and extrusion problems with the UHMWPE/HDPE (50/50) blend (Figure 8). The viscosity of the UHMWPE/PP (50/50) blend was much smaller, and the surface of the extrudate was smooth. The molten PP only partly penetrates the UHMWPE domains because of the poor miscibility between them. Most of the molten PP tends to locate between the UHMWPE particles, acting as a lubricant agent (Figure 2d). As the plasticating time increases, the PP will be more uniformly distributed between the UHMWPE particles and consequently its effect of PP on the viscosity reduction of the UHMWPE/PP (50/50) blend is expected to be more significant. This is confirmed by the rheological measurements (Figure 9).

As shown in Figure 8, addition of LDPE can also reduce the viscosity of UHMWPE. However, the viscosity of the UHMWPE/LDPE (50/50) blend is much higher than that of the UHMWPE/PP (50/50) blend, despite the fact that the viscosity of the PP was even higher than that of the LDPE. The parameter χ of the UHMWPE/LDPE (50/50) blends with small differences in branch contents (<30) is less than 6×10^{-4} . Thus, the small value of the interaction parameter χ induces more and more

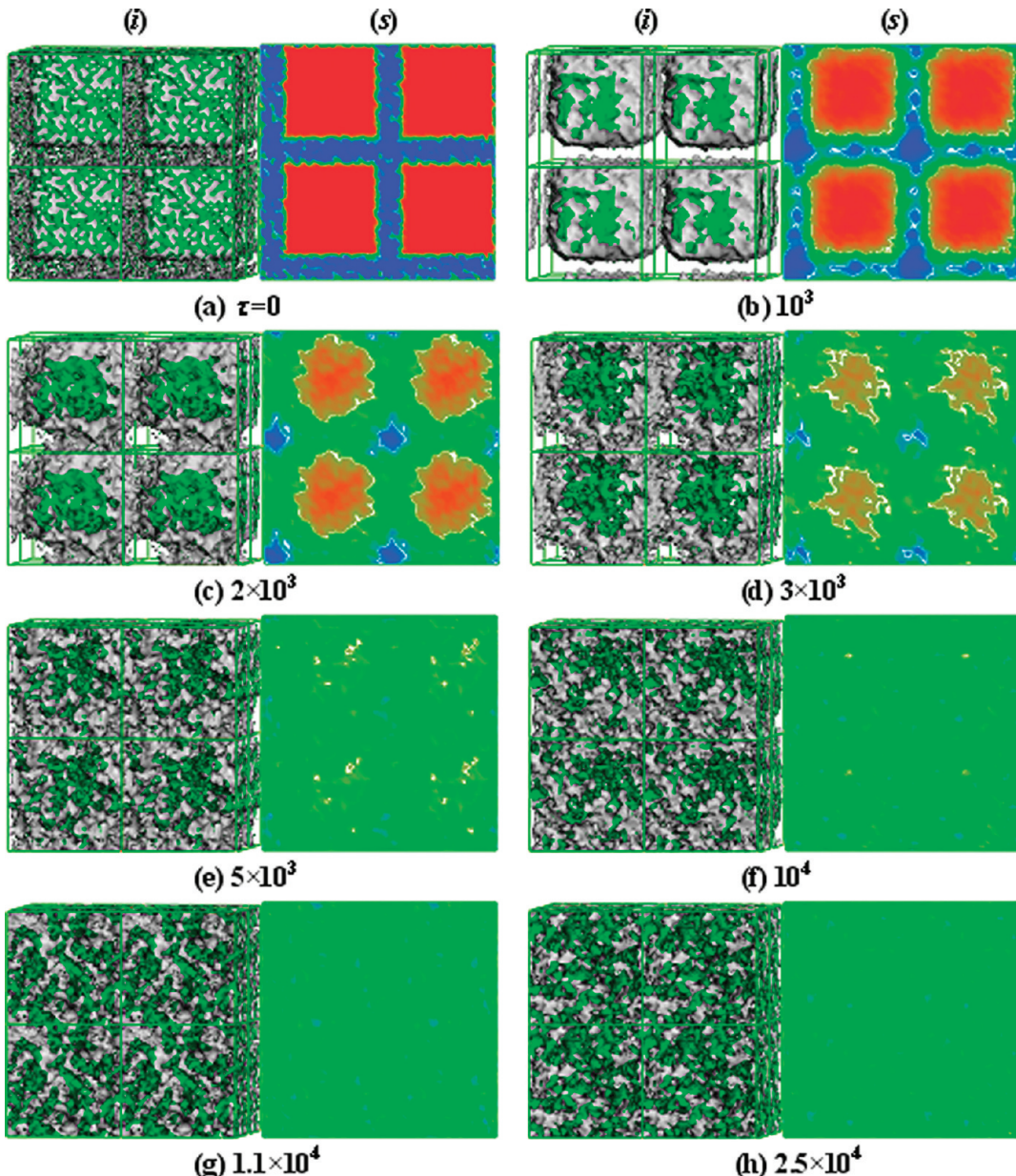


Figure 4. Snapshots of the UHMWPE/HDPE (50/50) blend simulated from a core–shell initial configuration (UHMWPE and HDPE are the core and shell, respectively): (i) time evolution of the isodensity surfaces of the HDPE; (s) corresponding slices. The others are the same as those in Figure 3.

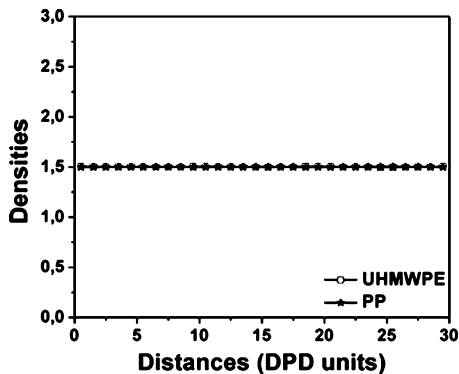


Figure 5. Density profiles of the UHMWPE/HDPE (50/50) blend after 1.1×10^4 time steps simulation from a core–shell initial configuration.

NMWP penetrates the UHMWPE phase and less and less NMWP will be available to form lubricating phases between the UHMWPE particles. Therefore, the apparent viscosity of the blend increases with increasing plasticating time (Figure 10).

HDPE and LDPE are superior to PP in disentangling the UHMWPE chains owing to their better miscibility with the UHMWPE. On the other hand, PP is found to be much more efficient in decreasing the viscosity of UHMWPE than HDPE and LDPE. Therefore, formation of the lubricating phase between the UHMWPE particles upon addition of NMWP might be the dominant factor of its viscosity reduction. In what follows, the phase diagrams of the UHMWPE/NMWP blends are studied in order to better understand the effects of the interaction parameter χ , content, and molecular weight of NMWP on the lubricating phase and viscosity of the blends.

4.3. Rheological Behavior Prediction Based on the Phase Diagram. Figure 11 shows the interaction parameter χ as a function of the volume fraction ϕ_{NMWP} for various N_1 (50, 250, and 1000) and fixed N_2 (11 600); N_1 and N_2 correspond to chain lengths of NMWP and UHMWPE, respectively (Table 1). The phase diagrams are calculated, and the binodal and spinodal curves together with the critical points are shown in Figure 11. In view of the fact that all of the blends of NMWP

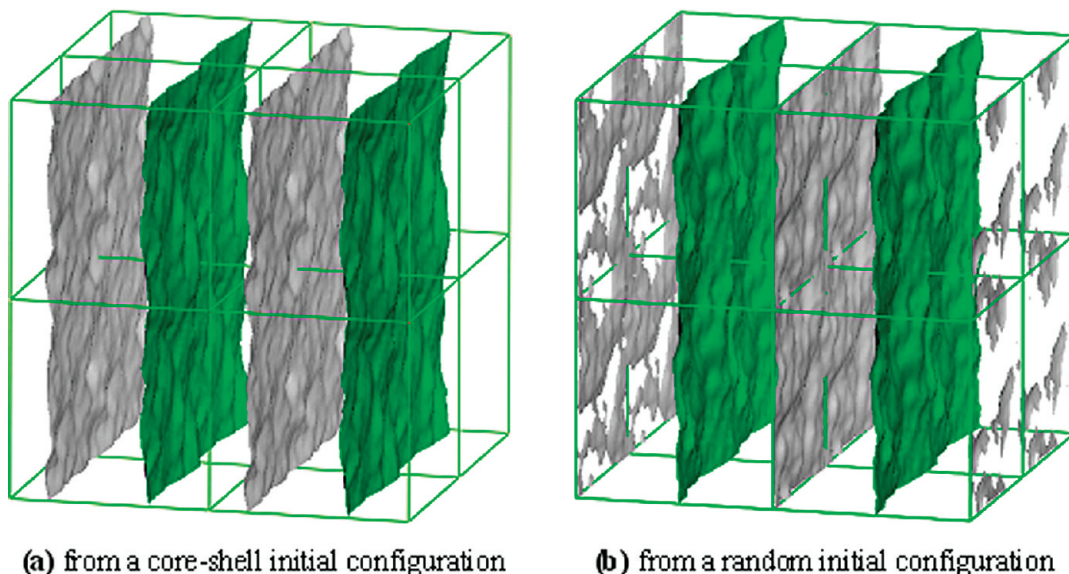


Figure 6. Isodensity surfaces of the PP for the UHMWPE/PP (50/50) blend with 4×10^5 steps. The outward surfaces of the PP phases are colored green, and the rest are the UHMWPE phases.

and UHMWPE with different N_1 possess similar properties, a representative one ($N_1 = 250$; $N_2 = 11\,600$) is plotted here to show the general properties of binary polymer systems with given N_2 . To obtain the UHMWPE/NMWP blends with different rheological behaviors and structures, some points (ϕ, χ) of the UHMWPE/NMWP blends should be located above the binodal curve while others should be below it. The composition of 50/50 is in accordance with the above-mentioned conditions. Besides, 50/50 is only one of the compositions that satisfies these conditions. The conclusions drawn from this composition will be valid for other compositions so long as they satisfy these conditions too. It is confirmed that the parameters χ of the UHMWPE/HDPE (50/50) blend and that of the UHMWPE/PP (50/50) blend lie below the binodal curve and above the spinodal one, respectively. Hence, the corresponding equilibrium states are characterized by the homogeneous phase and two-phase morphologies, respectively. This is in agreement with the DPD simulations and the SEM observations.

As shown in Figure 11, the composition of each of the phases in the UHMWPE/PP blend can be determined from the lever rule. The volume fractions of the UHMWPE in each of the phases are about 0 and 90%. This implies that about 10% of the PP may have penetrated the UHMWPE phase and nearly no UHMWPE is located in the PP phase, which is beneficial to the viscosity reduction of UHMWPE.

As stated in the Introduction, an excess in NMWP might bring about important deterioration in some of the most desirable properties of UHMWPE. Therefore, it is necessary to investigate the effect of the fraction of NMWP on the rheological behavior of the UHMWPE/NMWP blend. As shown in Figure 12, when the PP volume fraction is less than 10%, no remarkable viscosity reduction occurs. This is because under this composition UHMWPE and PP form a homogeneous phase (Figure 11). As the PP volume fraction increases, the UHMWPE/PP blend exhibits a very different rheological behavior, depending strongly on the shear rate.

The viscosity of the blend is reduced to a significant degree when the shear rate is in the range of 256.9 to 1999.8 s⁻¹ (Figure 12e–g). Moreover, when $\phi_{\text{PP}} \geq 0.1$ the flow is smooth and no pressure fluctuation has occurred. When the shear rate varies from 23.0 to 92.4 s⁻¹, there appear to be two distinct rheological behaviors for the UHMWPE/PP blend (Figure 12a–d). The

viscosity of the blends decreases dramatically with ϕ_{PP} increasing from 0.1 to 0.3. This is because when $\phi_{\text{PP}} > 0.1$, about 10% PP would penetrate the UHMWPE phase and the rest forms a lubricating phase between the UHMWPE particles. An increase in the PP volume fraction leads to an increase in the amount of the PP available for forming that lubricating phase and consequently a reduction in the apparent viscosity of the blend. Nevertheless, the viscosity of the blends varies only slightly when the PP volume fraction exceeds 30%. This could be explained by the fact that 30% PP is enough to form the lubrication phase between UHMWPE particles. An excess in PP can only increase the thickness but not the area of the lubrication phase. The range of $0.3 \geq \phi_{\text{PP}} \geq 0.1$ is thus called composition-sensitive region, CSR, of low shear rates for the UHMWPE/PP blends.

Consequently, for a given UHMWPE/NMWP blend with fixed parameter χ and molecular weight of each component, the optimum composition ratio should be located in the CSR of the blends for low shear rates and ensure the parameter χ to be above but close to the corresponding binodal curve for high shear rates. It is worth noting that all the ranges for the low shear rate, high shear rate, and CSR rigorously depend on the rheological behavior of the blend. From Figure 12, the metastable region for the UHMWPE/PP blend is located in the corresponding CSR. Thus, the CSR, which may not always be easily measured in practice, can be approximately replaced by the metastable region provided that the viscosity of the blend is low enough for processing within the metastable region.

Figure 11 shows that an increase in the parameter χ favors formation of a two-phase structure. At the same time, it accelerates the rate with which the NMWP molecules migrate toward the surface of the blends during processing. As a result, the NMWP can no longer effectively act as a lubricant agent between UHMWPE particles. Moreover, the interfacial thickness will decrease, leading to worse mechanical properties. Therefore, for UHMWPE/NMWP blends with fixed content and molecular weight of each component, the optimum value of the parameter χ should be above but close to the corresponding binodal curve. Figure 11 also shows that for a polymer blend with fixed parameter χ , both the corresponding binodal and spinodal curves shift downward with increasing N_1 , indicating that increasing

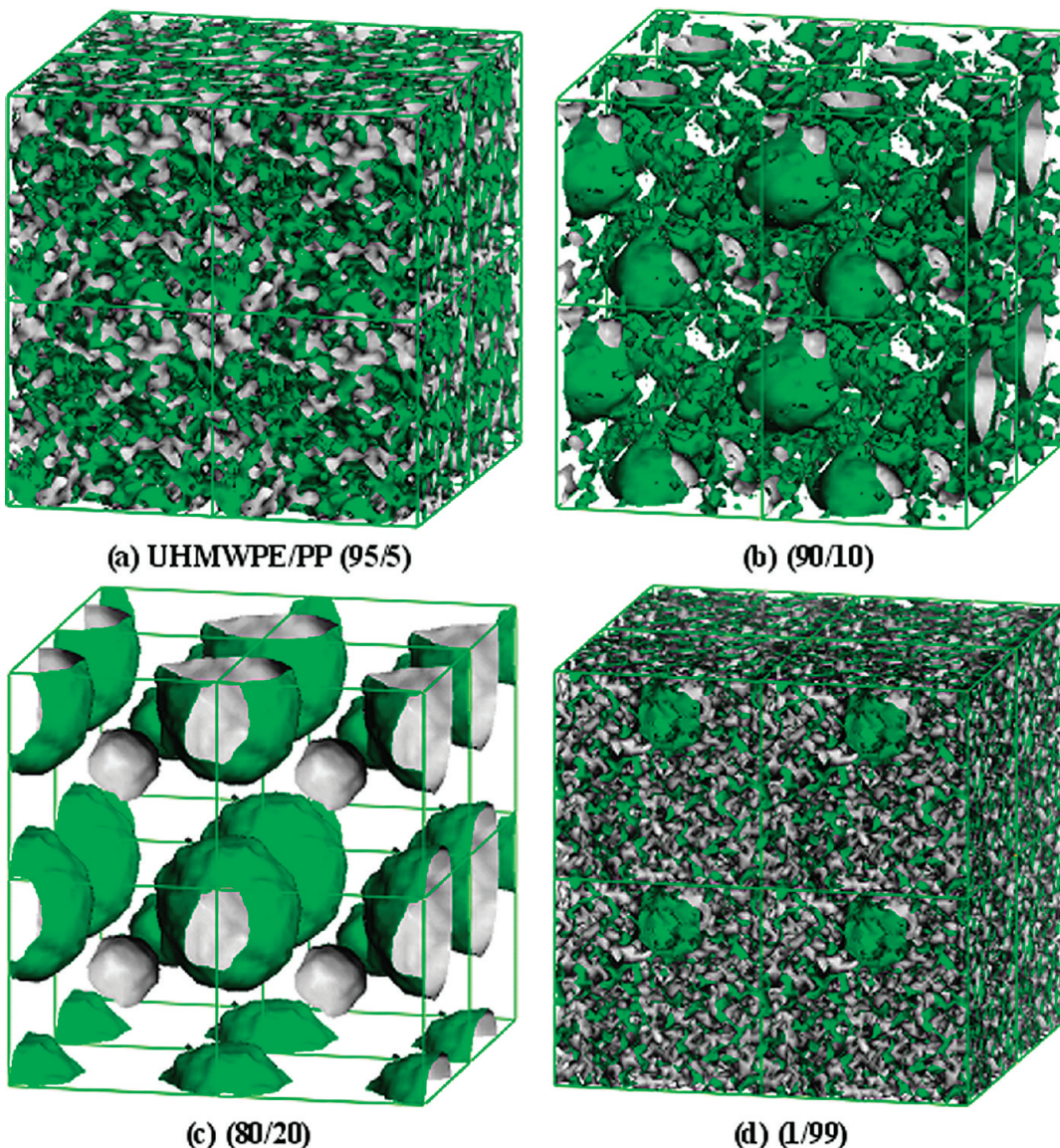


Figure 7. Snapshots of the UHMWPE/PP blends simulated from a core–shell initial configuration. The outward surfaces of the PP phases are colored green, and the rest are the UHMWPE phases.

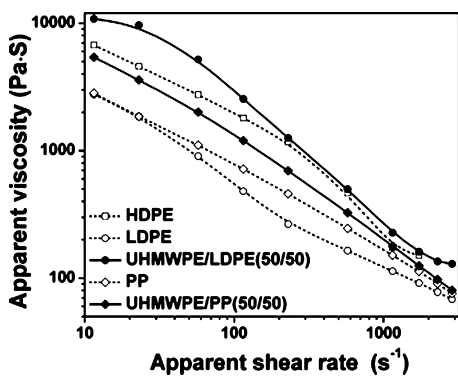


Figure 8. Plot of the logarithm of the apparent viscosity versus the logarithm of the apparent shear rate, and both blends were mixed for 15 min.

the molecular weight of NMWP in a certain range can improve the processability of UHMWPE owing to formation of a lubricating phase between the UHMWPE particles (Figure 11a–c).

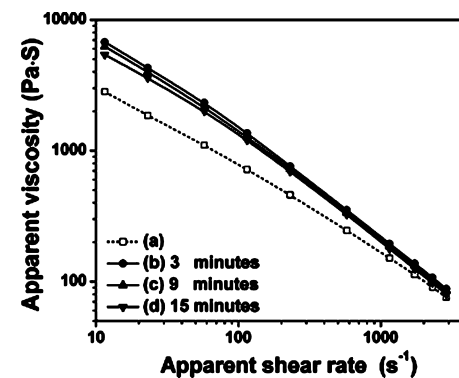


Figure 9. Plot of the logarithm of the apparent viscosity versus the logarithm of the apparent shear rate for (a) PP and (b–d) UHMWPE/PP (50/50) blend.

5. Conclusion

In this work, we investigated the effects of NMWP on the morphologies and rheological behaviors of the UHMWPE blends by experimental measurements and theoretical predictions.

HDPE and LDPE are better than PP to disentangle the UHMWPE molecules, but PP proved to be more effective than

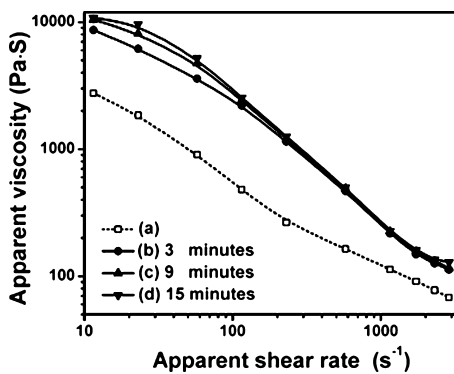


Figure 10. Plot of the logarithm of the apparent viscosity versus the logarithm of the apparent shear rate for (a) LDPE and (b–d) UHMWPE/LDPE blend (50/50).

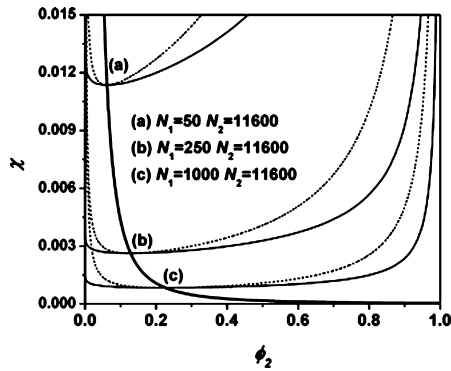


Figure 11. Binodals (solid curves) and spinodals (dashed curves) of polymer blends with fixed N_2 (11 600) and various N_1 : (a–c) critical points. The bold solid curve is composed of the critical points.

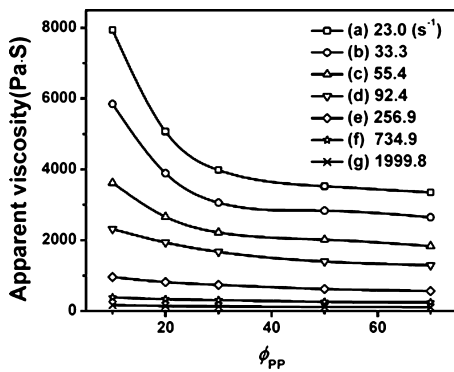


Figure 12. Plot of the apparent viscosity versus the PP fraction for the UHMWPE/PP (50/50) blend mixed for 3 min.

HDPE and LDPE in decreasing the viscosity of the UHMWPE/LDPE blends in our research. Therefore, formation of the lubrication phase between the UHMWPE particles with addition of NMWP might be the dominant factor of the viscosity reduction.

A phase diagram is adopted here to investigate the effects of the interaction parameter χ , molecular weight, and content of each component on the lubrication phase and the viscosity of blends. Results show that for a given UHMWPE/NMWP blend with fixed parameter χ and molecular weight of each of the components, the optimum composition ratio should be located in the CSR of the blends for low shear rates. The parameter χ is above but close to the corresponding binodal curve for high shear rates.

The phase diagram also shows that for a polymer blend with fixed parameter χ , both the corresponding binodal and spinodal

curves shift downward with increasing N_1 , which indicates that increasing the molecular weight of NMWP in a certain range can improve the processability of blends because of the appearance of the lubrication phase between the UHMWPE particles.

It is hoped that these results would also be proved suitable for researching the rheological behaviors on other nonpolar ultrahigh molecular weight polymer blends.

Acknowledgment

This work was supported by the National Basic Research Program of China (2005CB623800), the National Natural Science Foundation of China (51003067), the Fundamental Research Funds for the Central Universities, and the China Scholarship Commission.

Literature Cited

- Oral, E.; Beckos, C. G.; Muratoglu, O. K. Free Radical Elimination in Irradiated UHMWPE through Crystal Mobility in Phase Transition to the Hexagonal Phase. *Polymer* **2008**, *49*, 4733–4739.
- Prever, E. B.; Crova, M.; Costa, L.; Dallera, A.; Camino, G.; Gallinaro, P. Unacceptable Biodegradation of Polyethylene in Vivo. *Biomaterials* **1996**, *17*, 873–878.
- Furmanski, J.; Pruitt, L. A. Peak Stress Intensity Dictates Fatigue Crack Propagation in UHMWPE. *Polymer* **2007**, *48*, 3512–3519.
- Wen, J. P.; Yin, P.; Zhen, M. H. Friction and Wear Properties of UHMWPE/nano-MMT Composites under Oilfield Sewage Condition. *Mater. Lett.* **2008**, *62*, 4161–4163.
- Ranade, R. A.; Wunder, S. L.; Baran, G. R. Toughening of Dimethacrylate Resins by Addition of Ultra High Molecular Weight Polyethylene (UHMWPE) Particles. *Polymer* **2006**, *47*, 4318–4327.
- Zwijnenburg, A.; Pennings, A. J. Longitudinal Growth of Polymer Crystals from Flowing Solutions III. Polyethylene Crystals in Couette Flow. *Colloid Polym. Sci.* **1976**, *254*, 868–881.
- Smith, P.; Lemstra, P. J. Ultra-High-Strength Polyethylene Filaments by Solution Spinning/Drawing. *J. Mater. Sci.* **1980**, *15*, 505–510.
- Zuo, J. D.; Zhu, Y. M.; Liu, S. M.; Jiang, Z. J.; Zhao, J. Q. Preparation of HDPE/UHMWPE/MMWPE Blends by Two-Step Processing Way and Properties of Blown Films. *Polym. Bull.* **2007**, *58*, 711–722.
- Vadhar, P.; Kyu, T. Effects of Mixing on Morphology, Rheology, and Mechanical Properties of Blends of Ultra-High Molecular Weight Polyethylene with Linear Low-Density Polyethylene. *Polym. Eng. Sci.* **1987**, *27*, 202–210.
- Lee, E. M.; Oh, Y. S.; Ha, H. S.; Kim, B. K. Rheological Properties of UHMWPE/iPP Blends. *Polym. Adv. Technol.* **2009**, *20*, 1121–1126.
- Xie, M. J.; Li, H. L. Viscosity Reduction and Disentanglement in Ultrahigh Molecular Weight Polyethylene Melt: Effect of Blending with Polypropylene and Poly(ethylene glycol). *Eur. Polym. J.* **2007**, *43*, 3480–3487.
- Li, X. M.; Zhou, W.; Jiang, T. Preparation of UHMWPE/PLA Blends. *China Synth. Resin Plastics* **2008**, *25*, 11–15.
- Kyu, T.; Vadhar, P. Cocrystallization and Miscibility Studies of Blends of Ultrahigh Molecular Weight Polyethylene with Conventional Polyethylenes. *J. Appl. Polym. Sci.* **1986**, *32*, 5575–5584.
- Liu, G. D.; Li, H. L. Extrusion of Ultrahigh Molecular Weight Polyethylene Under Ultrasonic Vibration Field. *J. Appl. Polym. Sci.* **2003**, *89*, 2628–2632.
- Hoogerbrugge, P. J.; Koelman, J. M. V. A. Simulating Microscopic Hydrodynamic Phenomena with Dissipative Particle Dynamics. *Europhys. Lett.* **1992**, *19*, 155–160.
- Koelman, J. M. V. A.; Hoogerbrugge, P. J. Dynamic Simulations of Hard-Sphere Suspensions under Steady Shear. *Europhys. Lett.* **1993**, *21*, 363–368.
- Español, P.; Warren, P. B. Statistical Mechanics of Dissipative Particle Dynamics. *Europhys. Lett.* **1995**, *30*, 191–196.
- Groot, R. D.; Warren, P. B. Dissipative Particle Dynamics: Bridging the Gap between Atomistic and Mesoscopic Simulation. *J. Chem. Phys.* **1997**, *107*, 4423–4436.
- Groot, R. D.; Madden, T. J. Dynamic Simulation of Diblock Copolymer Microparticle Separation. *J. Chem. Phys.* **1998**, *108*, 8713–8725.
- Kong, Y.; Manke, C. W.; Madden, W. G. Effect of Solvent Quality on the Conformation and Relaxation of Polymers via Dissipative Particle Dynamics. *J. Chem. Phys.* **1997**, *107*, 592–603.

- (21) Rekvig, L.; Kranenburg, M.; Vreede, J.; Hafskjold, B.; Smit, B. Investigation of Surfactant Efficiency Using Dissipative Particle Dynamics. *Langmuir* **2003**, *19*, 8195–8205.
- (22) Tsige, M.; Grest, G. S. Molecular Dynamics Simulation of Solvent-Polymer Interdiffusion: Fickian diffusion. *J. Chem. Phys.* **2004**, *120*, 2989–2996.
- (23) Lee, W. J.; Ju, S. P.; Wang, Y. C. Molecular Dynamics of a Short-Range Ordered Smectic Phase Nanoconfined in Porous Silicon. *J. Chem. Phys.* **2007**, *127*, 064902–064912.
- (24) Yang, H.; Li, Z. S.; Lu, Z. Y.; Sun, C. C. Computer Simulation Studies of the Miscibility of Poly(3-hydroxybutyrate)-Based Blends. *Eur. Polym. J.* **2005**, *41*, 2956–2962.
- (25) Flory, P. J. *Principles of Polymer Chemistry*; Cornell University: New York, 1942.
- (26) Huggins, M. L. Some Properties of Solutions of Long-Chain Compounds. *J. Phys. Chem.* **1942**, *46*, 151–158.
- (27) Qian, C. B.; Mumby, S. J.; Eichinger, B. E. Phase Diagrams of Binary Polymer Solutions and Blends. *Macromolecules* **1991**, *24*, 1655–1661.
- (28) Rubinstein, M.; Colby, R. H. *Polymer Physics*; Oxford University Press: New York, 2003.
- (29) Hildebrand, J. H. *The Solubility of Non-Electrolytes*; Reinhold: New York, 1936.
- (30) Case, F. H.; Honeycutt, J. D. Will My Polymers Mix? Methods for Studying Polymer Miscibility. *Trends Polym. Sci.* **1994**, *2*, 259–266.
- (31) Liu, D. H.; Zhong, C. L. Cooperative Self-Assembly of Nanoparticle Mixtures in Lamellar Diblock Copolymers: A Dissipative Particle Dynamics Study. *Macromol. Rapid Commun.* **2006**, *27*, 458–462.
- (32) Groot, R. D.; Madden, T. J.; Tildesley, D. J. On the Role of Hydrodynamic Interactions in Block Copolymer Microphase Separation. *J. Chem. Phys.* **1999**, *110*, 9739–9750.
- (33) Groot, R. D. Electrostatic Interactions in Dissipative Particle Dynamics - Simulation of Polyelectrolytes and Anionic Surfactants. *J. Chem. Phys.* **2003**, *118*, 11265–11278.
- (34) Özen, A. S.; Sen, U.; Atilgan, C. Complete Mapping of the Morphologies of Some Linear and Graft Fluorinated co-Oligomers in an Aprotic Solvent by Dissipative Particle Dynamics. *J. Chem. Phys.* **2006**, *124*, 064905–064914.
- (35) Liu, D. H.; Zhong, C. L. Multicompartment Micelles Formed From Star-Dendritic Triblock Copolymers in Selective Solvents: A Dissipative Particle Dynamics Study. *Polymer* **2008**, *49*, 1407–1413.
- (36) Jawalkar, S. S.; Aminabhavi, T. M. Molecular Modeling Simulations and Thermodynamic Approaches to Investigate Compatibility/Incompatibility of Poly(l-lactide) and Poly(vinyl alcohol) Blends. *Polymer* **2006**, *47*, 8061–8071.
- (37) Mark, J. E. *Polymer Data Handbook*; Oxford University Press: New York, 1999.
- (38) Rogers, D.; Hopfinger, A. J. Application of Genetic Function Approximation to Quantitative Structure-activity Relationships and Quantitative Structure-property Relationships. *J. Chem. Inf. Comput. Sci.* **1994**, *34*, 854–866.
- (39) Ray, S. S.; Maiti, P.; Okamoto, M.; Yamada, K.; Ueda, K. New Polylactide/Layered Silicate Nanocomposites. I. Preparation, Characterization, and Properties. *Macromolecules* **2002**, *35*, 3104–3110.
- (40) Sinha, R. S.; Okamoto, K.; Okamoto, M. Structure-Property Relationship in Biodegradable Poly(butylene succinate)/Layered Silicate Nanocomposites. *Macromolecules* **2003**, *36*, 2355–2367.
- (41) Fan, Z. G. J.; Williams, M. C.; Choi, P. A Molecular Dynamics Study of the Effects of Branching Characteristics of LDPE on Its Miscibility with HDPE. *Polymer* **2002**, *43*, 1497–1502.

Received for review April 25, 2010
Revised manuscript received September 24, 2010
Accepted September 28, 2010

IE100959F